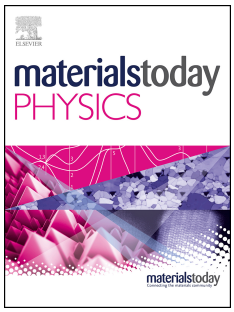

A Synergy of Strain Loading and Laser Radiation in Determining the High-Performing Electrical Transports in the Single Cu-Doped SnSe Microbelt

Yunzhi Zheng, Xiao-Lei Shi, Hualei Yuan, Siyu Lu, Xianlin Qu, Wei-Di Liu, Lihua Wang, Kun Zheng, Jin Zou, Zhi-Gang Chen

PII: S2542-5293(20)30022-5

DOI: https://doi.org/10.1016/j.mtphys.2020.100198

Reference: MTPHYS 100198

To appear in: *Materials Today Physics*

Received Date: 2 February 2020

Revised Date: 19 February 2020

Accepted Date: 20 February 2020

Please cite this article as: Y. Zheng, X.-L. Shi, H. Yuan, S. Lu, X. Qu, W.-D. Liu, L. Wang, K. Zheng, J. Zou, Z.-G. Chen, A Synergy of Strain Loading and Laser Radiation in Determining the High-Performing Electrical Transports in the Single Cu-Doped SnSe Microbelt, *Materials Today Physics*, https://doi.org/10.1016/j.mtphys.2020.100198.

Table of Content

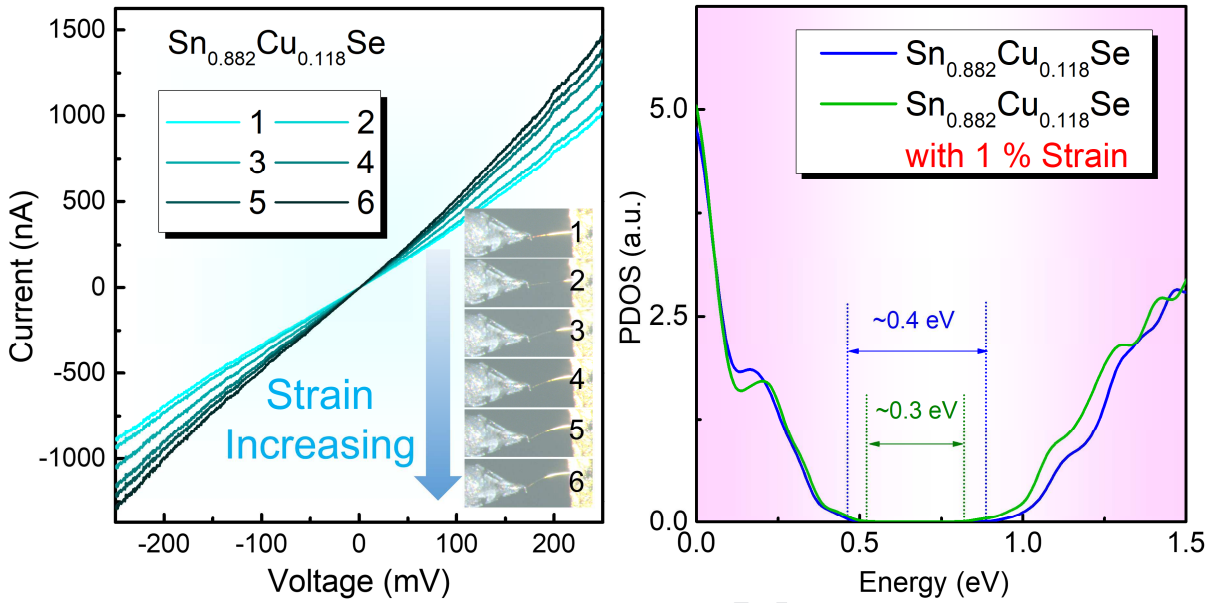

A Synergy of Strain Loading and Laser Radiation in Determining the High-Performing Electrical Transports in the Single Cu-Doped SnSe Microbelt

Yunzhi Zheng,[1,a] Xiao-Lei Shi,[2,3,a] Hualei Yuan,[1] Siyu Lu,[4] Xianlin Qu,[1] Wei-Di Liu,[3] Lihua Wang,[1] Kun Zheng,[1,] Jin Zou,[3,5] and Zhi-Gang Chen[2,3,*]*

[1] Beijing Key Lab of Microstructure and Property of Solids, Institute of Microstructure and Property of Advanced Materials, Beijing University of Technology, Beijing, 100124, China;

[2] Centre for Future Materials, University of Southern Queensland, Springfield Central, QLD, 4300, Australia;

[3] School of Mechanical and Mining Engineering, University of Queensland, Brisbane, QLD, 4072, Australia;

[4] College of Chemistry and Molecular Engineering, Zhengzhou University, Zhengzhou, 450001, China;

[5] Centre for Microscopy and Microanalysis, University of Queensland ,Brisbane QLD 4072 Australia

[a] These authors contribute equally to this work.

Corresponding Author

* Kun Zheng: kunzheng@bjut.edu.cn.

* Zhi-Gang Chen: zhigang.chen@usq.edu.au; zhigang.chen@uq.edu.au.

Abstract

Semiconducting microbelts are key components of the thermoelectric micro-devices, and their electrical transport properties play significant roles in determining the thermoelectric performance. Here, we report heavily Cu-doped single-crystal SnSe microbelts as potential candidates employed in thermoelectric micro-devices, fabricated by a facile solvothermal route. The considerable Cu-doping concentration of ~11.8 % up to the solubility contributes to a high electrical conductivity of ~416.6 S m^{-1} at room temperature, improved by one order of magnitude compared with pure SnSe (38.0 S m^{-1}). Meanwhile, after loading ~1 % compressive strain and laser radiation, the electrical conductivity can be further improved to ~601.9 S m^{-1} and ~589.2 S m^{-1}, respectively, indicating great potentials for applying to thermoelectric micro-devices. Comprehensive structural and compositional characterizations indicate that the Cu^{+} doping state provides more hole carriers into the system, contributing to the outstanding electrical conductivity. Calculations based on first-principle density functional theory reveal that the heavily doped Cu lowers the Fermi level down into the valence bands, generating holes, and the 1 % strain can further reduce the bandgap, strengthening the ability to release holes, and, in turn, leading to such an excellent electrical transport performance. This study fills the gaps of finding novel materials as potential candidates employed in the thermoelectric micro-devices and provides new ideas for micro/nanoscale thermoelectric material design.

Keywords: tin selenide, electrical transport performance, Cu-doping, strain loading, laser radiation.

1. Introduction

With the aggravation of energy and environmental crises, achieving higher energy utilization efficiency has become one of the most effective ways to solve the problems. Thermoelectric materials can realize the direct conversion between thermal and electric energies, which are expected to be widely applied in the field of waste heat recovery and power generation [1-4]. To evaluate the thermoelectric conversion efficiency of materials, a dimensionless figure-of-merit ZT has been defined as $ZT = S^2\sigma T/\kappa$, where S is the Seebeck coefficient, σ is the electrical conductivity, T is the absolute temperature, and κ is the thermal conductivity, respectively [5-9]. A high ZT requires a high power factor ($S^2\sigma$) and a low κ, and a high σ is of significance to ensure a high thermoelectric power generation [10-12]. To achieve a high σ, a high carrier concentration n (for electrons) or p (for holes) is needed according to $\sigma = ne\mu$ *or* $pe\mu$, where e is the electrical charge and μ is the carrier mobility [13-15], respectively. For most of the thermoelectric materials, to achieve high ZTs, their pristine n or p values need further tuning to achieve a high σ and in turn, a high $S^2\sigma$ [16], as shown in **Figure S1** in Supporting Information, and doping and alloying are two effective ways to achieve this goal [3, 17-19].

As a key member in the thermoelectric family, microscale thermoelectric devices (or thermoelectric micro-devices) have been paid considerable attention in recent years due to their full potentials for employing in continuous power generation and refrigeration for various applications [2, 20], such as the thermoelectric windows embedded with micro-generators that can produce electricity by collecting the heat from outdoor [21, 22], and the thermoelectric micro-coolers that can cool the processors during working in electronic devices [23]. Microscale single-crystal semiconductors are suitable candidates for employing in these thermoelectric

micro-devices, and their electrical transport properties (mainly σ) play significant roles in determining the thermoelectric performance [24, 25]. However, restricted by the considerable crystal dimensions up to several hundred micrometers for applying to microdevices, exploring ideal single crystal thermoelectric materials with both suitable crystal size and high thermoelectric performance are historically tricky [7, 26]. To solve this issue, SnSe has been considered as a good candidate due to their controllable size of synthesized single crystals, abundance in raw materials, environmentally friendly feature, high cost-effectiveness, and excellent thermoelectric performance resulted from their suitable band-gap values of ~0.9 eV and ultra-low κ derived from their specific anharmonic layered crystal structure, as shown in **Figure S2** [6, 27-29]. However, the synthesized SnSe single crystals by transitional aqueous solution routes such as hydrothermal or solvothermal methods were typical microplates due to their orthorhombic crystal nature [28-33], which need further cutting into microbelts for applying to microdevices; at the same time, due to the low p of pristine SnSe, σ from these microplates still need further improvement such as doping to achieve a high thermoelectric power generation [34]. Besides, the loading of stress (or strain) should also influence σ of SnSe microcrystals because the strain can change the atomic spacing and in turn alter the band structure, leading to the change of electrical properties of materials. Since any materials should be stressed during their applications, and since band structures of any semiconductors change under strain, it is critically important to clarify the band change of thermoelectric materials during their service [34]. However, very few experimental studies have been performed on the influence of strain loading on σ of SnSe microscale single crystals. Furthermore, whether there are any other potential assistant techniques such as laser radiation that can further improve σ of SnSe microscale single crystals is unknown.

In this study, we fabricated heavily Cu-doped single-crystal SnSe microbelts as potential candidates targeting thermoelectric micro-devices through a facile solvothermal route. The Cu-doped SnSe can induce morphologies transferring from rectangular microplates to microbelts, which is suitable for direct use in the micro-devices, avoiding any further processing. A considerable Cu solubility of ~11.8 % in SnSe contributed to a high σ of ~416.6 S m^{-1} at room temperature, improved by one order of magnitude compared with pure SnSe microplates (38.0 S m^{-1}). It is found that, after loading ~1 % compressive strain and laser radiation, σ can be further improved to ~601.9 S m^{-1} and ~589.2 S m^{-1}, respectively, indicating great potentials for them to be used as thermoelectric micro-devices. To study the fundamental mechanism of heavily Cu-doping on improving the electrical transport performance of SnSe, morphological, structural, and compositional characterizations including X-ray diffraction (XRD), scanning electron microscopy (SEM), transmission electron microscopy (TEM), energy dispersive spectroscopy (EDS), spherical aberration-corrected scanning transmission electron microscopy (Cs-STEM), and X-ray photoelectron spectroscopy (XPS) were comprehensive investigated, and the results indicate that both Cu^{2+} and Cu^{+} doping states were found in heavily Cu-doped SnSe, and the Cu^{+} doping state can provide more hole carriers into the system, contributing to an improved p and in turn an enhanced σ. Besides, we performed detailed calculations based on first-principle density functional theory (DFT), and the results indicate that the doped Cu enables the Fermi level to move toward the valence band, and 1 % compressive strain can further reduce the bandgap, leading to such an excellent electrical transport performance. This study fills the gaps of finding novel materials as potential candidates employed in the thermoelectric micro-devices and provides new ideas for micro/nanoscale thermoelectric material design.

2. Results and Discussion

Figure 1(a) shows the XRD patterns taken from synthesized pure SnSe, 2 % Cu-doped SnSe, and 11.8 % Cu-doped SnSe, respectively, in a 2θ range from 20° to 70°. The peak intensities were normalized for comparison. The Cu solubility of ~11.8 % was determined by the EDS when 20 at% Cu was chosen as a nominate doping concentration. As can be seen, all diffraction peaks can be exclusively indexed as the orthorhombic-structured SnSe with lattice parameters of a = ~1.14 nm, b = ~0.42 nm and c = ~0.44 nm and a space group of *Pnma* (JCPDS 48-1224) . The strongest peaks of 400* indicate that all products should possess significant {100} surfaces, making other peaks weak and hard to identify, similar to the bulk single crystals [6, 35, 36]. **Figure 1(b)** shows detailed 400* and 111* diffraction peaks in a 2θ range from 30° to 31.5°, magnified from **Figure 1(a)**, from which, with increasing the Cu-doping concentration, all peaks shift towards a higher 2θ. Since the sizes of Cu ions (0.077 nm for Cu^{+} and 0.074 nm for Cu^{2+}) are smaller than Sn ions (0.112 nm for Sn^{2+}) [37], the peak deviation indicates that Cu atoms are incorporated into the SnSe lattice. Besides, with increasing the Cu-doping concentration, 111* peaks become weaker, indicating the variation of crystal dimensions [6, 28].

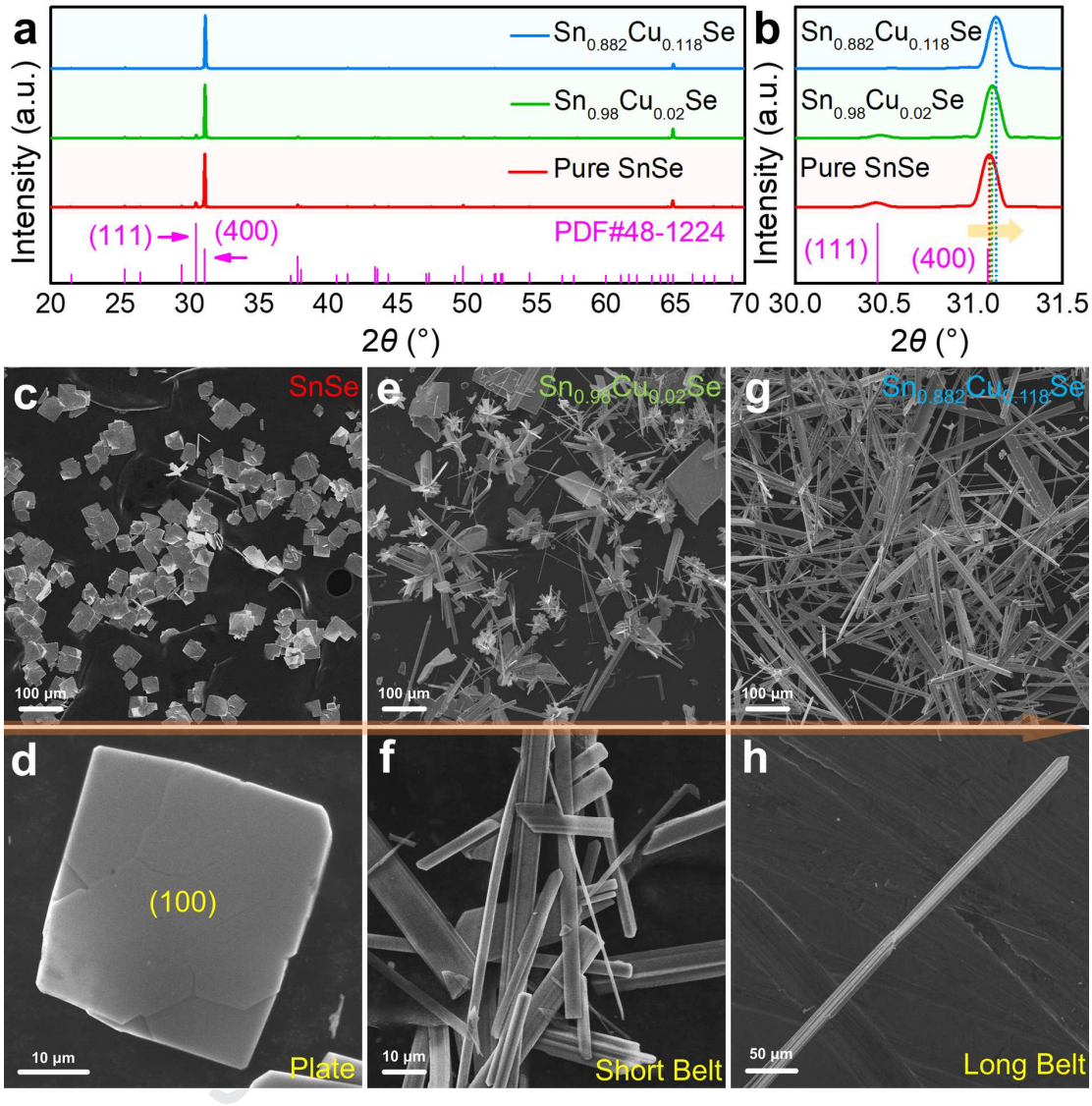

Figure 1. Structural and morphological characterizations on synthesized SnSe single crystals with different Cu-doping concentrations. (a) XRD patterns in a 2θ range from 20° to 70°, (b) magnified XRD patterns in a 2θ range from 30° to 31.5°. The peak intensities have been re-scaled for better comparison. (c) Low and (d) high magnification SEM images of SnSe microplates, (e) low and (f) high magnification SEM images of 2 % Cu-doped SnSe microbelts, and (g) low and (h) high magnification SEM images of 11.8 % Cu-doped SnSe microbelts.

To understand the morphological characteristics of our synthesized products, SEM investigation was performed. **Figures 1(c-d**) show low and high magnification SEM images of pure SnSe products, from which typical microplate-like products with an average dimension of ~50 μm can be observed. These significant {100} surfaces explain why 400* is the strongest peak, as shown in the XRD pattern. **Figures 1(e-f**) show SEM images of 2 at % Cu-doped SnSe products. Interestingly, the Cu-doping can transfer the shape of synthesized products from rectangular microplates to microbelts, indicating that Cu-doping may alter the growth direction of SnSe crystals. **Figures 1(g-h**) show SEM images of 11.8 % Cu-doped SnSe products. Surprisingly, with increasing the Cu-doping concentration, the dimensions of these microbelts were significantly enhanced, up to several hundreds of micrometers. Meanwhile, combined with the XRD results shown in **Figures 1(a-b)**, we confirm that the {100} are still the most significant surfaces on these microbelts. Corresponding optical images of our synthesized products can be seen in **Figure S3** for reference, and the refined lattice parameters as a function of Cu-doping concentration are shown in **Figure S4**, from which a shrinkage of unit cell can be observed by Cu-doping.

To clarify the Cu doping behaviour in SnSe, comprehensive TEM, EDS, and Cs-STEM investigations were performed. **Figures 2(a-c)** respectively show EDS spot analyses of three typical products, in which the corresponding EDS maps are also provided as insets. All the elements (Sn, Se, and Cu) are homogeneously distributed, indicating the homogeneous Cu doping in SnSe. **Figure S5** summarizes the comprehensive EDS spot data to confirm the ~11.8 % solubility of Cu in SnSe microbelts by the solvothermal route. **Figures 2(d-f)** show high-resolution TEM (HRTEM) images with insets of corresponding fast Fourier transform (FFT) patterns, all viewed along the [100] zone-axes. The FFT patterns were acquired from the entire

samples for Cu-doped microbelts. These patterns indicate typical orthorhombic structures for all products with significant {100} surfaces. Interestingly, with increasing the Cu-doping concentration, the lattice variations become more significant, probably derived from the doping of Cu in SnSe during solvothermal synthesis under high temperature and high vapor pressure [27, 29], which cause considerable lattice distortions. Meanwhile, after Cu-doping, multiple FFT patterns with slight deviations can be observed, indicating that the Cu-doping can probably result in local crystal bents, mainly derived from the severe lattice distortions. **Figures 2(g-i)** show Cs-STEM high-angle annular dark-field (HAADF) images viewed along the [100] directions, and a crystal structure of SnSe is shown in **Figure 2(g)** as inset [6, 15, 27, 29]. With increasing the Cu-doping concentrations, the non-uniform contrast and varied structural patterns become more significant (as the arrows showed), confirming the severe strains in the SnSe lattice by heavily Cu-doping, mainly derived from the ion difference between Sn and Cu.

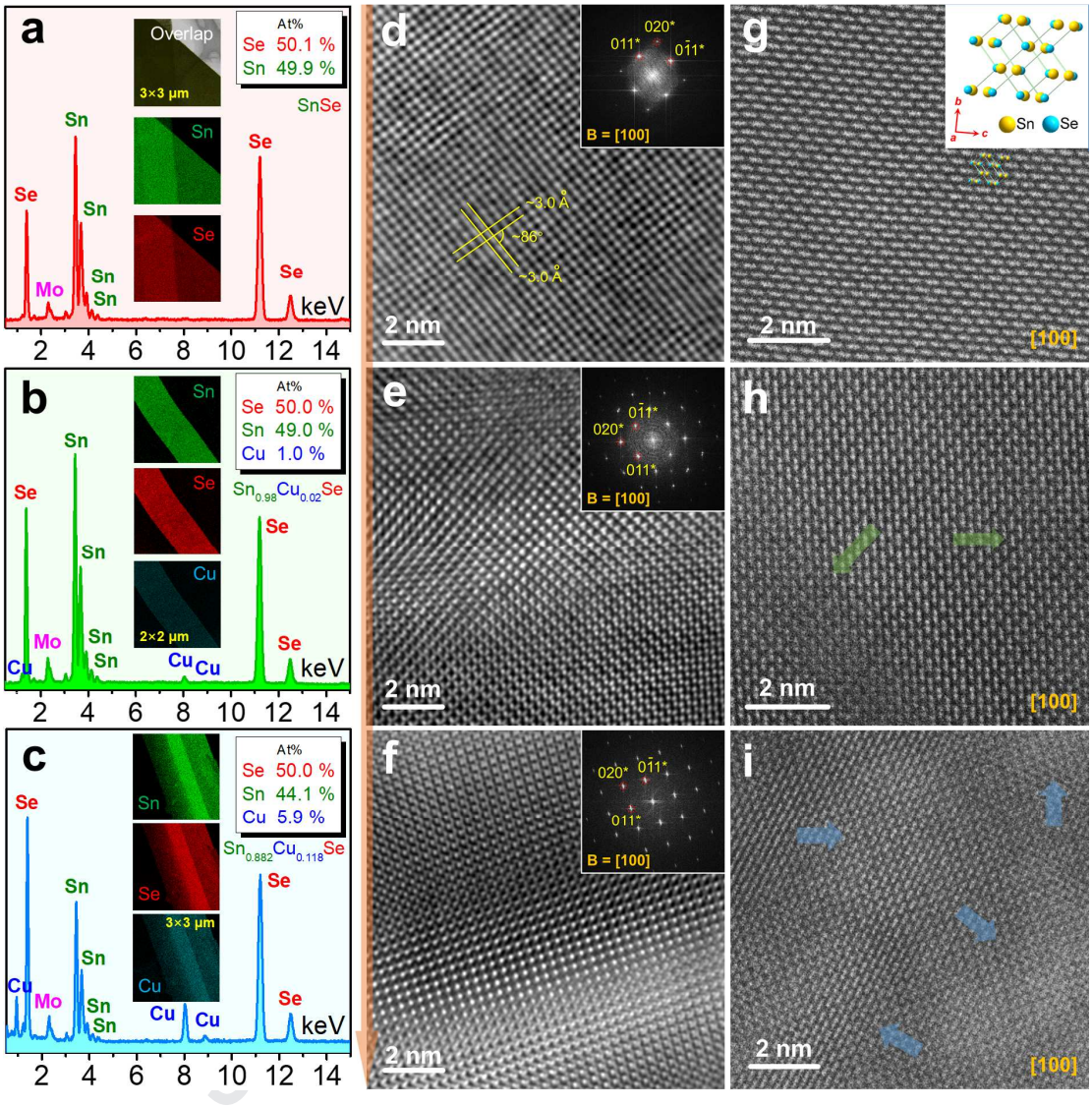

Figure 2. Compositional and structural characterizations on synthesized SnSe single crystals with different Cu-doping concentrations. EDS results of (a) SnSe microplates, (b) 2 % Cu-doped SnSe microbelts, and (c) 11.8 % Cu-doped SnSe microbelts, respectively, including spots and maps as inset. HRTEM images with inset of FFT patterns of (d) SnSe microplates, (e) 2 % Cu-doped SnSe microbelts, and (f) 11.8 % Cu-doped SnSe microbelts, respectively, viewed along the [100] directions. Cs-STEM-HAADF images of (g) SnSe microplates, (h) 2 % Cu-doped SnSe microbelts, and (i) 11.8 % Cu-doped SnSe microbelts, respectively, viewed along

the [100] directions. A crystal structure of SnSe (room temperature *Pnma* phase) is shown in (g) as inset [6, 15, 27, 29].

To understand the electrical transport performance of our synthesized SnSe single crystals with different Cu-doping concentrations, we employed an electrical test sample rod manufactured by Nanofactory, as schematically shown in **Figure 3(a)**, in which the sample rod is driven by a piezoelectric ceramic to realize the movement of the W tip in three dimensions. By controlling the movement of the W tip, the current-voltage (I-V) curve of different samples under specific stress/strain loading can be realized. **Figure 3(b)** shows an optical image of the setup of the electrical measurement when a SnSe microbelt is connected by a Au wire. When the W tip contact with the sample, a closed circuit system is formed, and the corresponding I-V curve can be obtained. The maximum voltage loading range is from −10 to 10 V, and the piezoelectric drive system can drive the W tip to stress the SnSe belt, and the electrical transport performance under strain loading can then be evaluated. **Figure 3(c)** and **3(d)** show SEM images of 11.8 % Cu-doped SnSe microbelt and a pure SnSe microbelt, both with one end fixed on the gold wire, achieved by the focused ion beam (FIB) technique. The size of the selected SnSe microbelt is comparable to that of the W tip, leading to a good contact to form a closed loop.

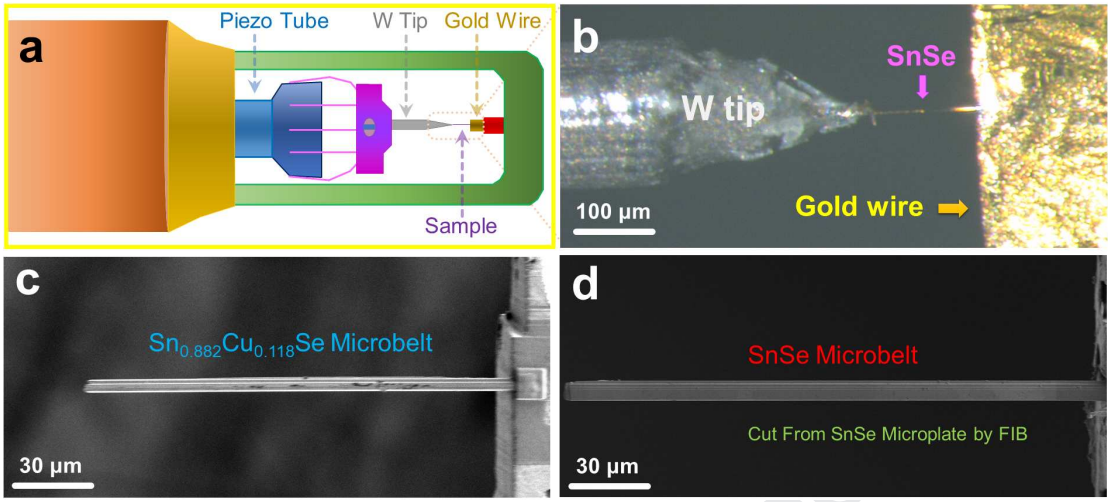

Figure 3. Illustration and characterizations of the electrical measuring system. (a) Schematic diagram and (b) optical microscopy image of the electrical measuring system. The SnSe sample is fixed on the Au wire and contacts with a tungsten needle tip connected to the piezoelectric ceramic to form an electrical closure system, and the corresponding current-voltage (I-V) curve can be obtained by loading the voltage. SEM images taken from (c) a 11.8 % Cu-doped SnSe microbelt and (d) a pure SnSe microbelt-like sample cut from the microplate by FIB.

Figure 4(a) shows optical images of the SnSe microbelts with different Cu-doping concentrations during I-V curve testing by the electrical measuring system (with no stress loading). **Figure 4(b)** plots the achieved I-V curves with a fixed voltage loading range from −250 to 250 mV, from which linear I-V curves illustrate good ohmic contacts. It is clearly seen that with increasing the Cu-doping concentration, the slope of the I-V curve was greatly improved, and higher current values can be achieved under fixed voltage, indicating that the Cu-doping can significantly improve the electrical transport performance of SnSe microbelts. To further understand the potential mechanism of Cu-doping in improving the electrical transport

performance of SnSe, we performed XPS analysis to confirm the valence state of Cu in our Cu-doped SnSe microbelts, and the result of XPS spectra of Cu $2p_{1/2}$ is shown in the inset of **Figure 4(b)**. As can be seen, both Cu^{+} valence state *via* peak at 952.5 eV and Cu^{2+} valence state *via* peak at 954.5 eV can be confirmed, and Cu^{+} should play a dominant role in improving the electrical transport performance of SnSe due to the fact that Cu^{+} can provide more hole carriers when substituting Sn^{2+}, contributing to higher *p*. The XPS results of Sn and Se are shown in **Figure S6** for reference. To better evaluate the electrical transport performance of these microbelts, we derive their σ values by considering their sizes, using the formula of $\sigma = IL_b/VS_c$, where I is the current value, L_b is the length of the microbelts, V is the voltage value, and S_c is the cross-sectional area of the microbelts, respectively. When the microbelts have roughly round cross-sections, $S_c = \pi d_c^2/4$ was used, where d is the average diameter of the round cross-section; when the microbelts have roughly rectangular cross-sections, $S_c = a_c b_c$ was used, where a_c and b_c are the length and width values of the rectangular cross-section. **Table 1** shows the determined σ of SnSe microbelts with different Cu-doping concentrations. For each Cu-doping concentration, we measure five different microbelts to statistically gain their average value (σ_{ave}). It is clearly seen that with increasing the Cu-doping concentration, σ is significantly enhanced, and the ~11.8 % Cu-doping can result in a high σ_{ave} of ~416.6 S m^{-1} at room temperature, improved by one order of magnitude compared with pure SnSe (38.0 S m^{-1}). At the same time, σ of each microbelt under a given Cu-doping concentration is close to σ_{ave} (as indicated by the error bars shown in **Figure S7**), indicating that the electrical transport properties of the synthesized materials are stable.

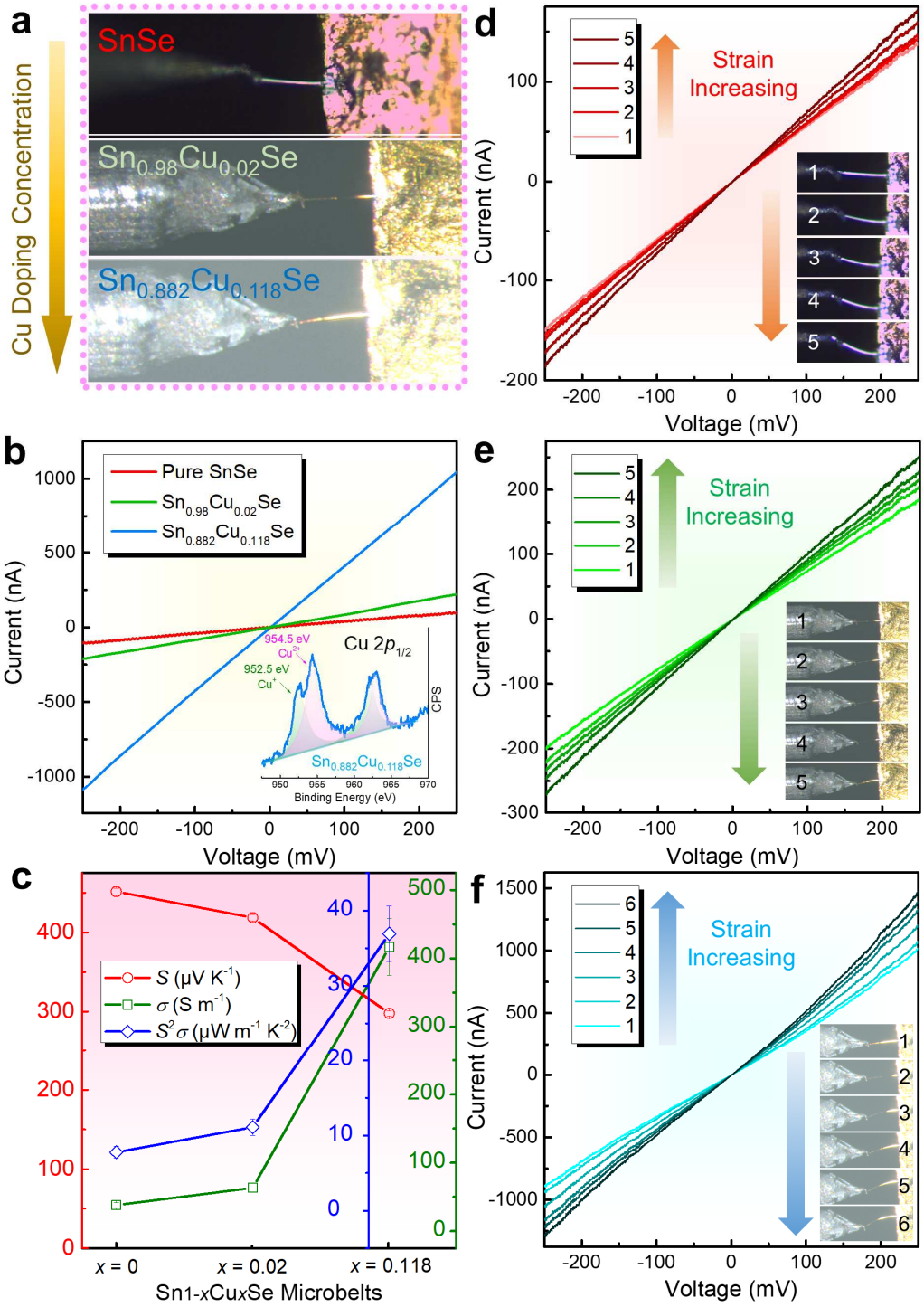

Figure 4. Evaluations of the electrical transport performance of SnSe microbelts with different Cu-doping concentrations. (a) Optical microscopy images of the microbelts, (b) I-V

curves with inset of the XPS result for Cu $2p_{1/2}$ taken from the 11.8 % Cu-doped SnSe microbelt, (c) determined electrical conductivity σ, evaluated Seebeck coefficient S, and estimated power factor $S^2\sigma$, I-V curves under increasing strains for (d) SnSe, (e) 2 % Cu-doped SnSe microbelts, and (f) 11.8 % Cu-doped SnSe microbelts, respectively. The arrows indicate the increasing of strains.

Table 1. Dimensions and the measured σ of SnSe microbelts.

No. of Microbelts	**Cu-doping level**	L_b **(μm)**	d_c **or** a_c **and** b_c **(μm)**	σ **(S m^{-1})**
1	0	31.14	1.550 and 0.209	40.67
2	0	72.71	2.706 and 0.219	52.14
3	0	51.74	4.072 and 0.259	19.77
4	0	39.34	1.639 and 0.234	44.97
5	0	33.02	1.810 and 0.239	32.55
σ_{ave}	0	—	—	**38.02**
1	2 %	70.79	1.713 and 0.246	57.91
2	2 %	49.15	2.098 and 0.215	70.69
3	2 %	57.84	1.974 and 0.254	61.77
4	2 %	41.09	1.755 and 0.263	50.78
5	2 %	39.17	3.029 and 0.259	75.44
σ_{ave}	2 %	—	—	**63.32**
1	11.8 %	223.01	1.645	475.51
2	11.8 %	134.62	1.353	422.83
3	11.8 %	74.46	1.111	462.37
4	11.8 %	123.83	1.424	355.79
5	11.8 %	57.41	1.201	366.65
σ_{ave}	11.8 %	—	—	**416.63**

To evaluate the thermoelectric potential of the as-fabricated microbelts for applying to microscale thermoelectric devices, we evaluate their power factor $S^2\sigma$. Although the direct measure of the Seebeck coefficient S is tricky for the microbelts, we can cold-press these microbelts into pellets and measure their room-temperature S as the references to evaluate their $S^2\sigma$, since the S of SnSe is weakly dependent on the measured directions (anisotropy) [6, 15, 27-29, 32-34, 38]. **Figure 4(c)** shows the determined σ, evaluated S, and estimated $S^2\sigma$ of SnSe microbelts with different Cu-doping concentrations. It is clearly seen that with increasing the Cu-doping level, the estimated $S^2\sigma$ of SnSe microbelts is significantly increased from ~7.8 μW m^{-1} K^{-2} for x = 0 to ~36.9 μW m^{-1} K^{-2} for x = 0.118, although the S is decreased from ~451.5 μV K^{-1} to 297.7 μV K^{-1}. These results indicate that heavily Cu-doped SnSe microbelts possess great potential for applying to microscale thermoelectric devices.

To understand the impact of strain on the electrical transport performance of our synthesized SnSe microbelts with different Cu-doping concentrations, we applied ~1 % stress on these microbelts during electrical testing, and **Figures 4(d-f)** show the measured I-V curves, respectively. The numbered optical images were shown as insets in these figures, indicating the stress loading process from 0 % to ~1 %, as illustrated by arrows. Since the higher stress loaded (such as >1%) may significantly increase the chance of damaging the SnSe microbelts (as shown in **Figure S8**) due to the fact that SnSe is a typical two-dimensional layer-structured semiconductor with a relatively low hardness [6, 33, 34], and since 1% is significant for their practical applications, we select the loaded strain up to ~1 % for all testing microbelts. As can be clearly seen in **Figure 4**, with increasing the stress loading, the slopes of the I-V curves become larger, indicating that appropriate stress applied to these microbelts can effectively improve their electrical transport performance. It is of interest to note that, under the same stress, the

improvement of σ for pure SnSe, 2 % Cu-doped SnSe, and 11.8 % Cu-doped SnSe were ~21.2 %, ~35.6 %, and ~44.5 %, respectively, indicating that the applied stress can lead to higher σ for higher Cu-doped belts, and a high σ_{ave} value of ~601.9 S m^{-1} has been achieved when ~1 % strain was applied to 11.8 % Cu-doped SnSe microbelts.

To understand the fundamental mechanism of improvement on the electrical transport performance of SnSe microbelts by heavy Cu-doping and stress loading, we performed detailed first-principle DFT calculations. **Figures 5(a-c)** show calculated band structures of SnSe, heavily Cu-doped SnSe, and heavily Cu-doped SnSe with 1 % strain, respectively, and **Figure 5(d)** compares the total DOS of the three samples. As can be clearly seen, the heavy Cu-doping can lower the Fermi level down into the valence bands of SnSe, which can significantly generate holes in the system, and in turn, boost the electrical transport property of SnSe. **Figures 5(e-g)** show corresponding partial DOSs of SnSe, heavily Cu-doped SnSe, and heavily Cu-doped SnSe with 1 % strain, respectively. Interestingly, the Cu-d orbital plays a significant role in strengthening the DOS of valence band, which is mainly derived from the +1 valence state of doped Cu. Such a considerable improvement in DOS of the valence state can also help strengthen the ability of releasing holes in the system. Notice that there is an abrupt increase in partial DOSs in the valence band of SnSe by Cu-doping. However, since the contribution of *d*-orbital of Cu in fact covers the entire valence band rather than only at the ~1.5 eV position (even though this position possesses the strongest peak), it is efficient enough to create extra holes in the systems by Cu-doping. **Figure 5(h)** compares the magnified total DOS of Cu-doped SnSe with and without 1 % strain. It is clear that after applying 1 % strain in the sample, the bandgap of Cu-doped SnSe can be further reduced from ~0.4 to ~0.3 eV, indicating a great enhancement

for the ability of generating holes and in turn, explaining why the strain-applied sample possesses such excellent electrical transport performance.

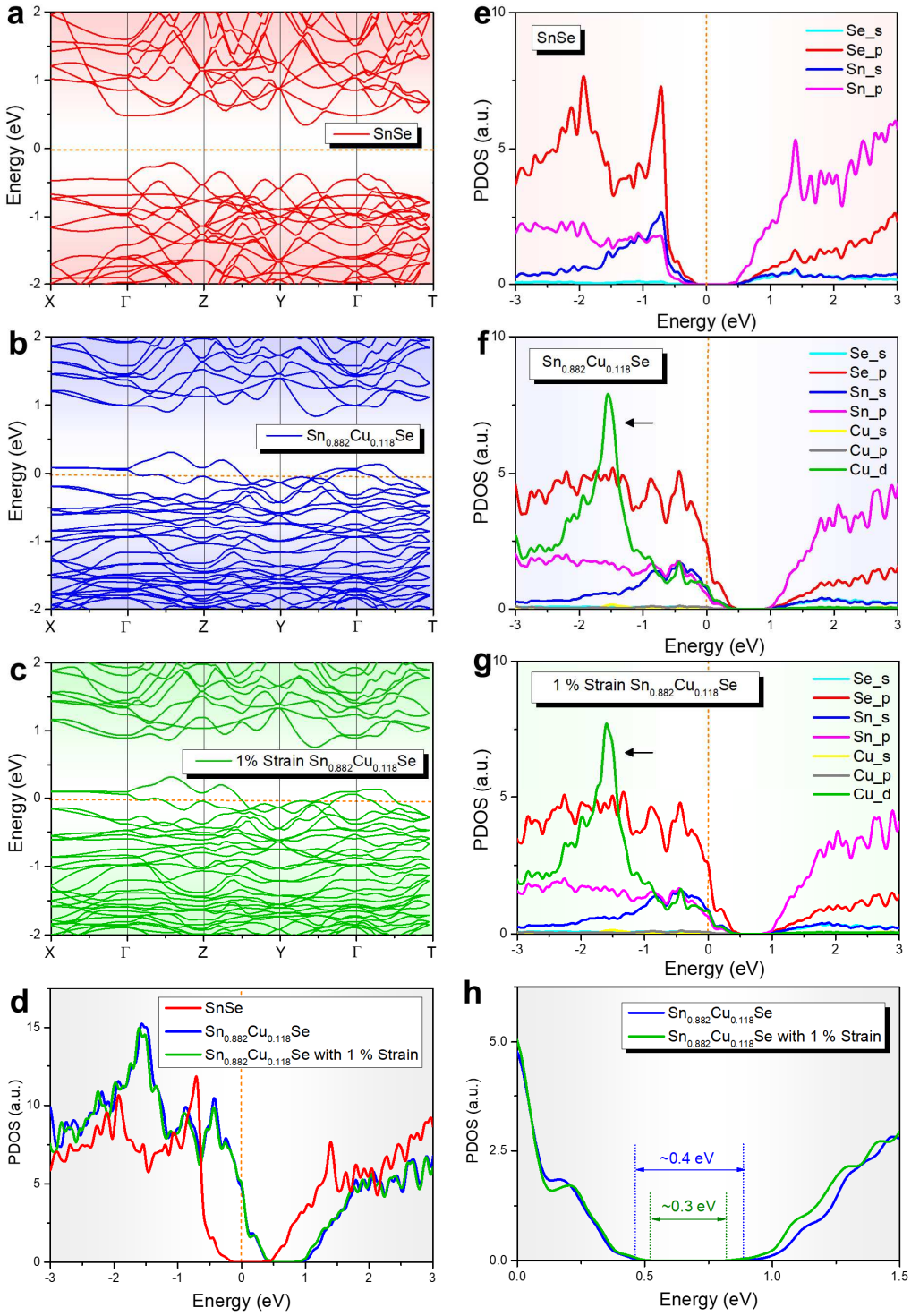

Figure 5. Calculations of SnSe single crystals. Calculated band structures of (a) SnSe, (b) heavily Cu-doped SnSe, and (c) heavily Cu-doped SnSe with 1 % strain, respectively; (d) comparison of total DOS of the three samples; corresponding partial DOS of (e) SnSe, (f) heavily Cu-doped SnSe, and (g) heavily Cu-doped SnSe with 1 % strain, respectively, and (h) magnified total DOS of Cu-doped SnSe with and without 1 % strain.

Furthermore, we applied laser radiation during the deformation testing. **Figures 6(a-c)** respectively shows the I-V curves of microbelts before and during laser irritations, in which with laser on, the slopes of the I-V curves become larger, indicating that laser radiation can further improve their electrical transport performance, probably owing to the effective activation of hole carriers by the laser radiation [39]. Also, with laser on, the improvement of σ for pure SnSe, 2 % Cu-doped SnSe, and 11.8 % Cu-doped SnSe were ~20.6 %, ~43.0 %, and ~41.4 %, respectively, indicating that higher Cu-doping concentration can contribute to higher σ under same laser radiation conditions, mainly derived from the higher p in heavily Cu-doped SnSe that more hole carriers can be activated by the laser, and a high σ_{ave} of ~589.2 S m^{-1} can be achieved when laser radiation was applied to 11.8 % Cu-doped SnSe microbelts, indicating great potentials for applying to thermoelectric micro-devices. **Figure 6(d)** shows the current variation of the 11.8 % Cu-doped SnSe microbelt when intermittently loading laser radiation under 10 mV, indicating that the improved σ by laser radiation is stable with high repeatability. It should be noticed that the sample doped with 2 % Cu shows the σ improvement slightly higher than that of 11.8 % Cu-doped sample. Such behavior may be derived from the fact that in 11.8 % Cu-doped SnSe, the free hole carriers have reached a considerable high carrier concentration p. In this situation, it may be not such sensitive to the laser that can produce more holes by the irritation, thus the extra

holes produced by laser irritation are limited, leading to a diminished effect of boosting the σ by laser irritation in ~11.8 % Cu-doped SnSe microbelts.

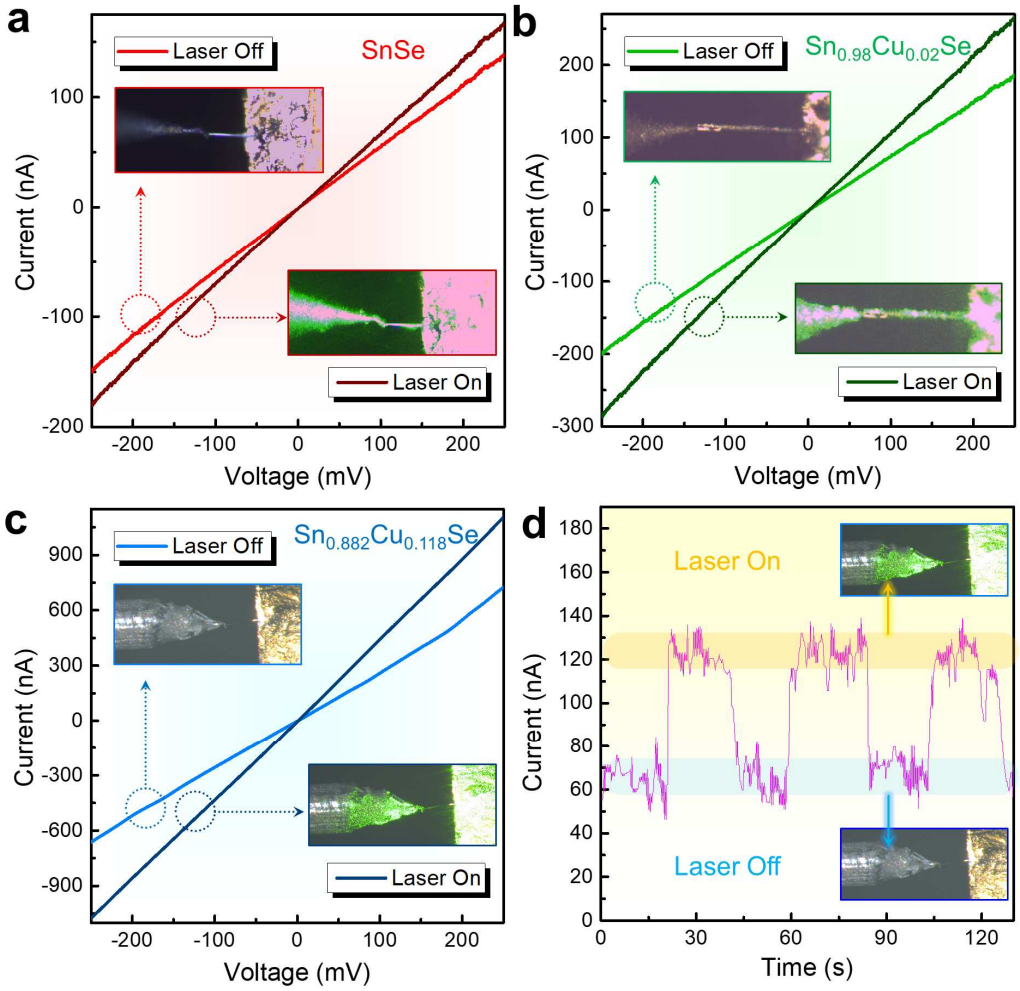

Figure 6. Influences of laser radiation on the electrical transport performance of SnSe microbelts. I-V curves of (a) pure SnSe, (b) 2 % Cu-doped SnSe, and (c) 11.8 % Cu-doped SnSe microbelts before and after laser radiation, and (d) current variation of the 11.8 % Cu-doped SnSe microbelt when intermittently loading laser radiation under 10 mV.

3. Summary

In this study, we fabricated heavily Cu-doped single-crystal SnSe microbelts as potential candidates for thermoelectric devices by a facile solvothermal route. Compared with pure SnSe microplates with a low electrical conductivity of ~38.0 S m^{-1}, the ~11.8 % Cu-doped SnSe microbelts exhibit ~ one order of magnitude improvement of the electrical conductivity, up to ~416.6 S m^{-1}. After loading ~1 % compressive strain and laser radiation, the electrical conductivity can be further improved to ~601.9 S m^{-1} and ~589.2 S m^{-1}, respectively, indicating great application potentials as thermoelectric devices. Detailed structural and compositional investigations confirm the co-existence of Cu^{2+} and Cu^{+} valence states in SnSe, which can provide more hole carriers, and lead to such higher electrical conductivity. DFT calculation indicates that the heavy Cu-doping lowers the Fermi level down into the valence bands, generating holes, and the applied 1 % strain can further reduce the bandgap, strengthening the ability to release holes and in turn, significantly improve the electrical transport performance. This study fills the gaps of finding novel materials as potential candidates employed in the thermoelectric micro-devices and provides new ideas for micro/nanoscale thermoelectric material design.

4. Experimental Details

Experimental details can be found in **Section 9** in Supporting Information.

Appendix A. Supplementary data

Supplementary data to this article can be found online at:

Acknowledgments

This work was financially supported by the National Natural Science Foundation of China (No. 11774016), Beijing Natural Science Foundation (Z180014) and Beijing Academic Outstanding Young Scientists Projects (BJJWZYJH01201910005018) and Australian Research Council. The Institute of Microstructure and Property of Advanced Materials and Microscopy Australia are acknowledged for providing characterization facilities.

References

[1] T. Zhu, Y. Liu, C. Fu, J.P. Heremans, J.G. Snyder, and X. Zhao, Adv. Mater. 29 (2017) 1605884.

[2] J. He and T.M. Tritt, Science 357 (2017) 9997.

[3] G. Tan, L.D. Zhao, and M.G. Kanatzidis, Chem. Rev. 116 (2016) 12123-12149.

[4] X. Shi and L. Chen, Nat. Mater. 15 (2016) 691-692.

[5] L. Yang, Z.-G. Chen, M.S. Dargusch, and J. Zou, Adv. Energy Mater. 8 (2017) 1701797.

[6] Z.-G. Chen, X. Shi, L.-D. Zhao, and J. Zou, Prog. Mater. Sci. 97 (2018) 283-346.

[7] R. Moshwan, L. Yang, J. Zou, and Z.-G. Chen, Adv. Funct. Mater. 27 (2017) 1703278.

[8] W.D. Liu, Z.G. Chen, and J. Zou, Adv. Energy Mater. (2018) 1800056.

[9] Y. Wang, L. Yang, X. Shi, X. Shi, L. Chen, M. Dargusch, J. Zou, and Z.-G. Chen, Adv. Mater. 31 (2019) 1807916.

[10] R. Chen, J. Lee, W. Lee, and D. Li, Chem. Rev. 119 (2019) 9260-9302.

[11] K. Zhao, P. Qiu, X. Shi, and L. Chen, Adv. Funct. Mater. (2019) 1903867.

[12] M. Hong, W. Lyu, Y. Wang, J. Zou, and Z.-G. Chen, J. Am. Chem. Soc. 142 (2020) 2672-2681.

[13] P. Jood, R.J. Mehta, Y. Zhang, G. Peleckis, X. Wang, R.W. Siegel, T. Borca-Tasciuc, S.X. Dou, and G. Ramanath, Nano Lett. 11 (2011) 4337-4342.

[14] M.K. Jana and K. Biswas, ACS Energy Lett. 3 (2018) 1315-1324.

[15] M. Jin, X.-L. Shi, T. Feng, W. Liu, H. Feng, S.T. Pantelides, J. Jiang, Y. Chen, Y. Du, J. Zou, and Z.-G. Chen, ACS Appl. Mater. Interf. 11 (2019) 8051-8059.

[16] M. Hong, T.C. Chasapis, Z.-G. Chen, L. Yang, M.G. Kanatzidis, G.J. Snyder, and J. Zou, ACS Nano 10 (2016) 4719-4727.

[17] Q. Zhang, F. Cao, W. Liu, K. Lukas, B. Yu, S. Chen, C. Opeil, D. Broido, G. Chen, and Z. Ren, J. Am. Chem. Soc. 134 (2012) 10031-10038.

[18] J.R. Sootsman, D.Y. Chung, and M.G. Kanatzidis, Angew. Chem. Int. Ed. 48 (2009) 8616-8639.

[19] L.D. Zhao, S. Hao, S.H. Lo, C.I. Wu, X. Zhou, Y. Lee, H. Li, K. Biswas, T.P. Hogan, C. Uher, C. Wolverton, V.P. Dravid, and M.G. Kanatzidis, J. Am. Chem. Soc. 135 (2013) 7364-7370.

[20] F.J. DiSalvo, Science 285 (1999) 703-706.

[21] S.B. Inayat, K.R. Rader, and M.M. Hussain, Sci. Rep. 2 (2012) 841.

[22] S.B. Inayat, K.R. Rader, and M.M. Hussain, Energy Technol. 2 (2014) 292-299.

[23] I. Chowdhury, R. Prasher, K. Lofgreen, G. Chrysler, S. Narasimhan, R. Mahajan, D. Koester, R. Alley, and R. Venkatasubramanian, Nat. Nano. 4 (2009) 235.

[24] Y. Wang, W.-D. Liu, X.-L. Shi, M. Hong, L.-J. Wang, M. Li, H. Wang, J. Zou, and Z.-G. Chen, Chem. Eng. J. (2019) 123513.

[25] D. Bao, J. Chen, Y. Yu, W. Liu, L. Huang, G. Han, J. Tang, D. Zhou, L. Yang, and Z.-G. Chen, Chem. Eng. J. 388 (2020) 124295.

[26] W. Liu, L. Yang, Z.-G. Chen, and J. Zou, Adv. Mater. (2020) 1905703.

[27] X.L. Shi, K. Zheng, W.D. Liu, Y. Wang, Y.Z. Yang, Z.G. Chen, and J. Zou, Adv. Energy Mater. 8 (2018) 1800775.

[28] X. Shi, A. Wu, W. Liu, R. Moshwan, Y. Wang, Z.-G. Chen, and J. Zou, ACS Nano 12 (2018) 11417-11425.

[29] X. Shi, A. Wu, T. Feng, K. Zheng, W. Liu, Q. Sun, M. Hong, S.T. Pantelides, Z.G. Chen, and J. Zou, Adv. Energy Mater. 9 (2019) 1803242.

[30] W.-H. Chen, Z.-R. Yang, F.-H. Lin, and C.-J. Liu, J. Mater. Sci. 52 (2017) 9728-9738.

[31] L. Huang, J. Lu, D. Ma, C. Ma, B. Zhang, H. Wang, G. Wang, D. Gregory, X. Zhou, and G. Han, J. Mater. Chem. A 8 (2020) 1394-1402.

[32] M. Dargusch, X.-L. Shi, X.Q. Tran, T. Feng, F. Somidin, X. Tan, W. Liu, K. Jack, J. Venezuela, H. Maeno, T. Toriyama, S. Matsumura, S.T. Pantelides, and Z.-G. Chen, J. Phys. Chem. Lett. 10 (2019) 6512-6517.

[33] X.-L. Shi, W.-D. Liu, A. Wu, V. Nguyen, H. Gao, Q. Sun, R. Moshwan, J. Zou, and Z.-G. Chen, InfoMat (2019) 1-15. DOI: 10.1002/inf2.12057.

[34] X.-L. Shi, X. Tao, J. Zou, and Z.-G. Chen, Adv. Sci. (2020) 1902923. DOI: 10.1002/advs.201902923.

[35] L.D. Zhao, S.H. Lo, Y. Zhang, H. Sun, G. Tan, C. Uher, C. Wolverton, V.P. Dravid, and M.G. Kanatzidis, Nature 508 (2014) 373-377.

[36] L.-D. Zhao, G. Tan, S. Hao, J. He, Y. Pei, H. Chi, H. Wang, S. Gong, H. Xu, and V.P. Dravid, Science 351 (2016) 141-144.

[37] J. Gao, H. Zhu, T. Mao, L. Zhang, J. Di, and G. Xu, Mater. Res. Bull. 93 (2017) 366-372.

[38] X. Shi, Z.-G. Chen, W. Liu, L. Yang, M. Hong, R. Moshwan, L. Huang, and J. Zou, Energy Storage Mater. 10 (2018) 130-138.

[39] A. Melnikov, I. Razdolski, T.O. Wehling, E.T. Papaioannou, V. Roddatis, P. Fumagalli, O. Aktsipetrov, A.I. Lichtenstein, and U. Bovensiepen, Phys. Rev. Lett. 107 (2011) 076601.

- 11.8 % Cu-doped SnSe single microbelt exhibits a high electrical conductivity of ~416.6 S m^{-1} at room temperature;
- 1 % compressive strain further boost the electrical conductivity of single microbelt up to ~601.9 S m^{-1};
- DFT calculations reveal the heavily doped Cu lowers the Fermi level of SnSe down into the valence bands, and 1 % strain further reduce the bandgap;
- Laser radiation improve the electrical conductivity of single microbelt up to ~589.2 S m^{-1}.

Sample CRediT author statement

Yunzhi Zheng: Methodology; Validation; Formal analysis; Investigation; Data Curation

Xiao-Lei Shi: Methodology; Software; Formal analysis; Investigation; Resources; Data Curation; Writing - Original Draft; Visualization

Hualei Yuan: Validation; Formal analysis; Investigation

Siyu Lu: Software; Resources

Xianlin Qu: Investigation; Formal analysis

Wei-Di Liu: Formal analysis

Lihua Wang: Resources; Funding acquisition

Kun Zheng: Conceptualization; Validation; Resources; Data Curation; Supervision; Project administration; Funding acquisition

Jin Zou: Formal analysis; Writing - Review & Editing

Zhi-Gang Chen: Conceptualization; Resources; Writing - Review & Editing; Supervision; Project administration; Funding acquisition

Declaration of interests

☒ The authors declare that they have no known competing financial interests or personal relationships that could have appeared to influence the work reported in this paper.

☐The authors declare the following financial interests/personal relationships which may be considered as potential competing interests: